Weierstraß-Institut
für Angewandte Analysis und Stochastik
Leibniz-Institut im Forschungsverbund Berlin e. V.

Preprint ISSN 0946 – 8633

Electronic states in a quantum well – nanobridge – quantum dot structure

Paul N. Racec [1,2], Leonid I. Goray [3,4]

submitted: December 17, 2013

[1] Weierstrass Institute
Mohrenstr. 39
10117 Berlin
Germany
E-Mail: paul.racec@wias-berlin.de

[2] National Institute of Materials Physics
PO Box MG-7
077125 Bucharest Magurele
Romania

[3] Saint Petersburg Academic University,
Khlopina 8/3
194021 St. Petersburg
Russia
lig@pcgrate.com

[4] Institute for Analytical Instrumentation, RAS,
Rizhsky Prospect 26
190103 St. Petersburg
Russia

No. 1898
Berlin 2013

2010 *Mathematics Subject Classification.* 65N30, 65Z05, 35P99.

2010 *Physics and Astronomy Classification Scheme.* 73.22.-f, 71.15.-m, 78.67.-n.

Key words and phrases. Nanobridge, hybrid bound states, optical matrix elements, cylindrical nanowire.

P. N. Racec acknowledges partial support from ERC-2010-AdG no. 267802 *AnaMultiScale* from European Research Council .

Edited by
Weierstraß-Institut für Angewandte Analysis und Stochastik (WIAS)
Leibniz-Institut im Forschungsverbund Berlin e. V.
Mohrenstraße 39
10117 Berlin
Germany

Fax: +49 30 20372-303
E-Mail: preprint@wias-berlin.de
World Wide Web: http://www.wias-berlin.de/

Abstract

Using the finite volume method we compute within effective mass approximation the single-particle eigenstates for electrons and holes in a InGaAs/GaAs quantum well – nanobridge – quantum dot structure. It is shown that hybrid states appear in this complex system. The interaction between the eigenvalues may be an explanation for the additional photoluminescence peak measured for inverted structures with smaller nanobridge lengths.

1 Introduction

The tunnel injection structures consist of a quantum well layer and a quantum dot layer separated by a spacer layer (i.e. host material playing the role of a barrier). They were developed in the last years for improving the performances of diode lasers [1, 2, 3, 4]. They have a special conduction band alignment, namely the ground state of the electron in the quantum well (QW) is between the ground and excited state in the quantum dot (QD) [1, 2, 3, 4]. In such a way, the electronic quantum dot ground state may be efficiently populated by tunnel injection from the quantum well ground state. The distance between these two active layers, QW as collector (injector) and QD as emitter, may be varied as an additional optimization parameter. Very recently the growth sequence of these structures was changed, such that the QD layer is grown first, followed by the barrier and after that by the QW [1, 4]. In these so-caled *inverted structures* was found that for distances $h < 5$ nm new features appear, like ultrafast carrier exchange [1] and an additional photoluminescence peak for a specific range of h values [4]. It was clearly shown that additional electronic states appear in this configuration and that distinct connections (called *nanobridges*) appear between the QW and QDs. In order to explain these features the electron and hole states were computed inside a cylinder with the same dimensions as the nanobridge [4]. There are also other attempts to model the electron and hole states inside such complex nanostructures. In Refs. [2, 3] two co-existing quantum-confined systems are considered (i.e. quantum well – wetting layer and quantum well – quantum dot) which can be treated as independent.

In this paper we present the electron and hole states of the combined system, i.e. quantum well, nanobridge and quantum dot computed within a three-dimensional model. It is considered that the nanobridge can also confine states within it. The strain is neglected. The In concentration within the nanobridge can be considered linearly distributed.

2 Model

2.1 Electronic structure

We consider a quantum well – nanobridge – quantum dot structure embedded in a "virtual" cylinder, as sketched in Fig. 1. The radius R and the height H of the cylinder are considered as free parameters in our model.

We assume the quantum dot as a truncated cone of height h_{QD}, with a (lower) base radius r_{QD} and the radius of the upper base equals the radius of the nanobridge. The nanobridge is considered as a cylinder with diameter D and height h.

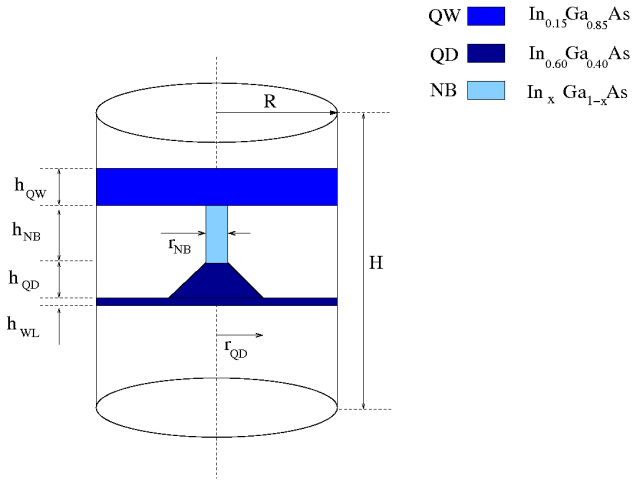

Figure 1: Sketch of a quantum well (QW) – nanobridge (NB) – quantum dot (QD) structure embedded in a "virtual" cylinder of a GaAs as host material.

The electronic structure is computed within single band effective mass approximation. In turn, the electronic states and the hole states are computed separately, as solutions of the Schrödinger-type equation for the envelope function

$$\left[-\frac{\hbar^2}{2}\nabla\cdot\left(\boldsymbol{M}(\mathbf{r})^{-1}\nabla\right)+V(\mathbf{r})\right]\Psi(\mathbf{r})=E\Psi(\mathbf{r}),\quad \mathbf{r}\in\Omega, \tag{1}$$

where $M(\mathbf{r})$ is the effective mass tensor (for electrons and holes, respectively) and $V(\mathbf{r})$ contains the (conduction and valence) band offsets of the heterostructure materials. The material parameters are taken from Refs. [5] and are summarized in Appendix A. The domain Ω is the virtual cylinder, on which surface Dirichlet boundary conditions are imposed. Due to the cylindrical symmetry, the solutions of Eq. (1) can be written as

$$\Psi(\mathbf{r})=\frac{e^{im\theta}}{\sqrt{2\pi}}\psi(z,r), \tag{2}$$

where the magnetic quantum number $m=0,\pm1,\pm2,...$ is integer and the z-axis is the cylinder axis. The eigenvalue problem (1) reduces in such a way to a series of two-dimensional eigenvalue problems [6]. Every eigenvalue problem, for a specific m value,

can be solved independently on the others using a finite volume method for cylindrical symmetric systems [7].

We compute nev eigenvalues for a specific m and index them by i. After computing for all m, with $m <$ mmax, the eigenvalues are sorted ascending, so that a pair (m, i) becomes an index n. The setup of the numerical parameters nev and mmax establishes the accuracy of the numerical calculations. Because we are interested in the bound states, i.e. energies lower than the conduction/valence band offsets, we consider

$$E^{(0)}_{\mathtt{nev}} > \Delta E_{c,v}, \qquad E^{(\mathtt{mmax})}_{i=1} \simeq E^{(\mathtt{mmax})}_{r,1} > \Delta E_{c,v}. \tag{3}$$

We consider the first confined energy in the r-direction $E^{(m)}_{r,1} = (\hbar^2/2m^*_r)(x_{m,1}/R)^2$ as a first approximation for the first eigenvalue for $m =$ mmax. In the above expression $x_{m,1}$ is the first root ($j = 1$) for the Bessel function of first kind $J_m(x)$ and m^*_r is the effective mass of the host material in the r-direction.

In the next subsections we will consider every subsystem separately and after that we will combine them.

2.2 Optical matrix elements

In order to describe the optical processes (i.e. absorption and emission of light) in semiconductor structures we follow Refs. [8, 9], where the interaction between photons and electrons in semiconductors is described in detail. The net transition rate that describes the absorption and emission processes can be computed using the Fermi's golden rule, in which the matrix elements of the minimal coupling perturbation Hamiltonian, called *optical matrix elements*, play the most important role. Using Coulomb gauge and the dipole (long wavelength) approximation, one can express them in terms of the momentum matrix elements or in terms of the electric dipole moment. We will follow the former variant.

For low-dimensional heterostructures, one often uses the envelope-function approximation, so that the single-particle wave function (for electrons or holes) may be written as [9, Eq. (1.52)]

$$\psi_{\boldsymbol{k}_0\nu\overline{\alpha}}(\boldsymbol{r}) = \sqrt{\Omega}\overline{\psi}_{\boldsymbol{k}_0\nu\overline{\alpha}}(\boldsymbol{r})\phi_{\boldsymbol{k}_0\nu}(\boldsymbol{r}), \tag{4}$$

where ν is the crystal band index and $\boldsymbol{k}_0$ is the wavevector at an extrema, i.e. minima or maxima, of the band ν. The envelope function $\overline{\psi}_{\boldsymbol{k}_0\nu\overline{\alpha}}$ is computed as a solution of the envelope-function equation and $\phi_{\boldsymbol{k}_0\nu}(\boldsymbol{r})$ is the (three-dimensional) Bloch state. In such a way, the optical matrix elements for nanostructures are given by the formula [9, Ch. 1.2.2, Eq. (1.55.)]

$$H'_{\nu'\overline{\alpha'},\nu\overline{\alpha}} \propto p^{\mathrm{env}}_{\nu,\overline{\alpha'}\overline{\alpha}}\delta_{\nu\nu'} + f^{\mathrm{env}}_{\nu'\overline{\alpha'},\nu\overline{\alpha}}p^{\mathrm{bulk}}_{\nu\nu'}, \tag{5}$$

where

$$p^{\mathrm{env}}_{\nu,\overline{\alpha'}\overline{\alpha}} = \int_\Omega \overline{\psi}^*_{\nu\overline{\alpha'}}(\boldsymbol{r})[-i\hbar\Delta_A\overline{\psi}_{\nu\overline{\alpha}}(\boldsymbol{r})]d^3r \tag{6}$$

are dipole matrix elements between the envelope functions,

$$f^{\mathrm{env}}_{\nu'\overline{\alpha'},\nu\overline{\alpha}} = \int_\Omega \overline{\psi}^*_{\nu'\overline{\alpha'}}(\boldsymbol{r})\overline{\psi}_{\nu\overline{\alpha}}(\boldsymbol{r})d^3r \tag{7}$$

are corresponding overlap integrals, and $p^{\mathrm{bulk}}_{\nu\nu'} = p_{\mathbf{0},\nu\nu'}$ denote the bulk dipole matrix elements evaluated in $\boldsymbol{k}_0 = \mathbf{0}$ and related to the Kane energy E_p that is a material parameter. The indexes ν and ν' are the crystal band indexes, i.e. conduction- or valence-band. The generic index $\overline{\alpha}$ denotes a set of quantum numbers, whose nature (discrete or continuous) depends on the particular shape and dimensionality of the nanostructure under consideration. As one can see, there are two different types of optical processes [9, Ch. 1.2.2]

- the first term in (5) describes *intraband transitions*, i.e. processes within the same band ν. It describes absorption/emission processes in the infrared spectral region between different subbands $\overline{\alpha} \to \overline{\alpha'}$ of the same band ν.
- the second term in (5) describes processes connecting different bands $(\nu \neq \nu')$, called *interband transitions*. It describes absorption/emission processes around the visible spectral region, connecting valence- to conduction-band states.

We will consider the interband transitions, i.e. the second term, so that one computes the overlap integrals (7) between the envelope functions of electrons and holes, i.e. different bands. For cylindrical geometry, the envelope functions have the form [6]

$$\overline{\psi}_{\nu\overline{\alpha}}(\boldsymbol{r}) = \overline{\psi}_{\nu\overline{\alpha}}(r,\theta,z) = \frac{e^{im\theta}}{\sqrt{2\pi}}\Psi^{(\nu)}_{mn}(z,r), \tag{8}$$

so that the generic index $\overline{\alpha} = (mn)$ contains information about the magnetic quantum number m and the discrete index n due to the confinement inside the closed cylinder. The band index ν will be h for holes and e for electrons. The index $\boldsymbol{k_0} = 0$ has been omitted. The $\Psi^{(\nu)}_{mn}(\boldsymbol{r})$ are computed (up to a sign) within finite volume method. The overlap integral is computed over the whole cylinder. Due to the orthogonality relation

$$\frac{1}{2\pi}\int_0^{2\pi} e^{im\theta}e^{-im'\theta}d\theta = \delta_{mm'} \tag{9}$$

one has non-zero overlap integrals only for the same magnetic quantum number m for electrons and holes. This expresses an *optical selection rule* for cylindrical symmetric systems.

The absorption energies are computed as

$$\hbar\omega = E_e - E_h = E_{\mathrm{el.}} + E_g - \Delta E_c - (-E_{\mathrm{h.}} + \Delta E_v), \tag{10}$$

where $E_g = 1.424$ eV is the band gap of GaAs, $\Delta E_c = 0.423$ eV, $\Delta E_v = 0.332$ eV. The electron energies $E_{\mathrm{el.}}$ and the hole energies $E_{\mathrm{h.}}$ are computed as eigenvalues of the single-band Schrödinger type equation for the envelope functions. Anyway, for the optical matrix elements only the states below the band offsets are considered, so that $\hbar\omega \leq E_g$.

3 Results for electronic structure

3.1 Isolated cylindrical nanobridge with graded In concentration

In order to compare with the previous results [4] we consider the $In_xGa_{1-x}As$ nanobridge as an isolated cylinder with diameter D and length h embedded in a GaAs cylinder of radius R and length H as host material. In such a way, one takes into account the finite band offsets ΔE_c (ΔE_v) between the conduction (valence) bands of the nanobridge and of the host material. We consider the following parameters: $R = 5$ nm, $H = 30$ nm and the diameter of the nanobridge $D = 2$ nm. The nanobridge is always located in the middle of the virtual cylinder. Within our formalism we can consider a linearly graded In concentration in the cylindrical nanobridge

$$x(z) = x_0 + (z - z_0)\frac{x_1 - x_0}{z_1 - z_0}, \tag{11}$$

where z_0 and z_1 are the z-coordinates of the begin and the end of the cylindrical nanobridge, and x_0 and x_1 are the In concentration at the begin and the end of the cylindrical nanobridge, respectively. We consider $x_0 = 0.15$ and $x_1 = 0.6$, while the length of the cylindrical nanobridge $h = z_1 - z_0$ is considered of different values from 1 to 10 nm.

For every triangular finite element (i) the material parameters are computed corresponding to the In concentration at the z-coordinate of the circumcenter $z_U^{(i)}$. We consider the minimum of the valence/conduction band offset as reference energy. So that, the potential energy due to the heterostructure is for electrons

$$V_e(z,r) = \begin{cases} \Delta E_c(x = 0.60) - \Delta E_c(x(z)), & r < r_{NB},\ z_0 < z < z_1 \\ \Delta E_c(x = 0.60), & \text{otherwise} \end{cases} \tag{12}$$

and for holes

$$V_h(z,r) = \begin{cases} \Delta E_v(x = 0.60) - \Delta E_v(x(z)), & r < r_{NB},\ z_0 < z < z_1 \\ \Delta E_v(x = 0.60), & \text{otherwise} \end{cases} \tag{13}$$

A sketch of the heterostructure potential on the axis of the cylinder (i.e. $r = 0$) is presented in Fig. 2.

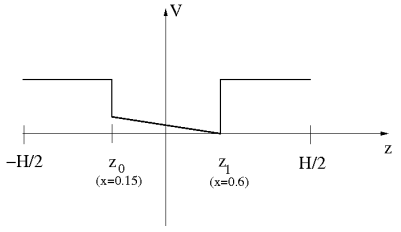

Figure 2: Sketch of the heterostructure potential for a cylindrical nanobridge with graded In concentration.

Fig. 3 shows the first four eigenenergies for electrons and holes inside a $In_xGa_{1-x}As$ cylindrical nanobridge with linearly graded In concentration, as a function of the cylinder height h. The number of grid points in the z-direction is $N_z = 600$ and in the r-direction $N_r = 100$, so that the mesh grid is $h_z = h_r = 0.05$ nm. On the same plot are presented the eigenenergies for constant In concentration. In order to compare the data, the results for $x = 0.15$ were shifted with $\Delta E = 0.302$ eV for the electron energies and with $\Delta E = 0.237$ eV for the hole energies, respectively.

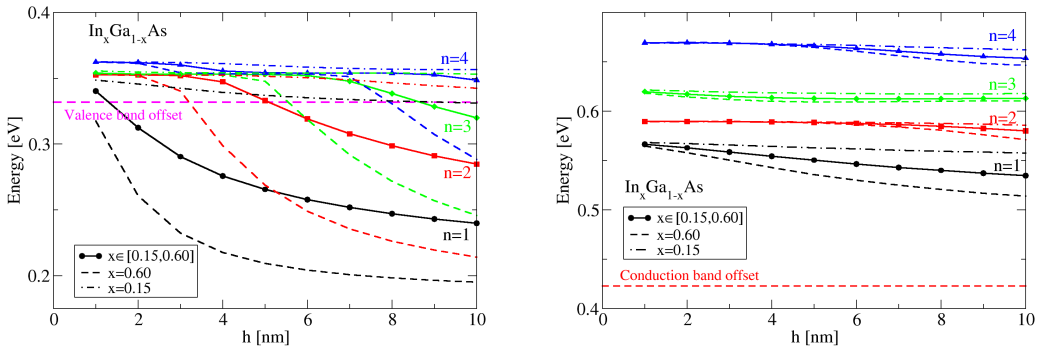

(a) Hole energies.

(b) Electron energies.

Figure 3: First four eigenenergies (solid lines with symbols) for electrons and holes inside a $In_xGa_{1-x}As$ cylindrical nanobridge vs. height h ($D = 2$ nm). The In concentration x is considered linearly graded from 0.15 until 0.6. The dashed lines indicate the values for $x = 0.60$ while the dot-dashed lines indicate the values for $x = 0.15$.

As expected [4], there are confined hole states inside the nanobridge, but there are no confined electron states. The variations of the eigenenergies with the In concentration is stronger for holes as for electrons.

The localization probabilities, i.e. $|\Psi(E_n; z, r)|^2$ in [nm$^{-3/2}$] in the domain $(zr) \in [-15, 15] \times [0, 5]$, are represented in Fig. 4 as color maps for the first four hole states for $h = 10$ nm. As one can observe, the states are strongly localized to the end of the nanobridge with higher In content. The state $n = 4$ is weaker localized inside the nanobridge because its energy is above the valence band offset.

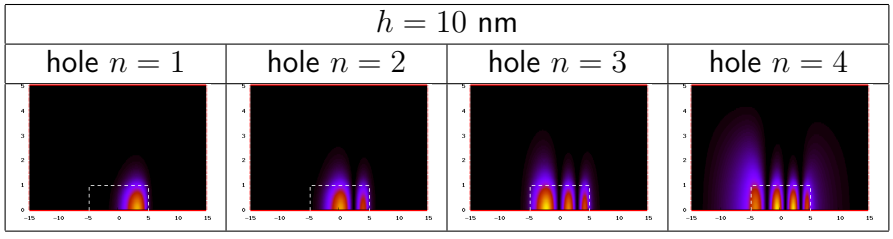

Figure 4: Localization probabilities as (zr)-maps for the first four hole eigenstates for $h = 10$ nm. Bright means high values. The white lines sketch the domain of the nanobridge.

The eigenenergies of the hole states in Fig. 3(a) above the valence band offset, which remain almost constant, correspond to the states that are localized outside the nanobridge but inside the "virtual" cylinder. They are due to Dirichlet boundary conditions on its surface.

3.2 Isolated quantum dot

We present in this section the hole and electron states in a truncated cone $In_{0.6}Ga_{0.4}As$ quantum dot. The radii are $r_1 = r_{NB} = 1$ nm and $r_2 = r_{QD} = 9$ nm and the height of the truncated cone is $h_{QD} = 4$ nm. The dot is considered alone into the "virtual" cylinder with dimensions $R = 15$ nm and $H = 16$ nm. The numerical parameters are $\texttt{mmax} = 8$ and $\texttt{nev} = 10$ for electrons and $\texttt{nev} = 30$ for holes. The number of grid points are specified on the plot.

The hole and electron eigenvalues are presented in Fig. 5, where also their distribution over magnetic quantum number m is shown. There are more hole states than electron states due to larger effective mass of the hole. It is clear that inside the quantum dot there are at least two electron bound states. The sequence of the magnetic quantum numbers m in the eigenvalues depends on the dimensions of the quantum dot, i.e. the ratios h_{QD}/r_2 and h_{QD}/r_1, and on the effective mass. The sequence of the m values in the lowest eigenvalues differs for electrons and holes because of the finite confinement potential, i.e. finite band offsets and also due to the difference of the effective masses in the quantum dot and in the host material.

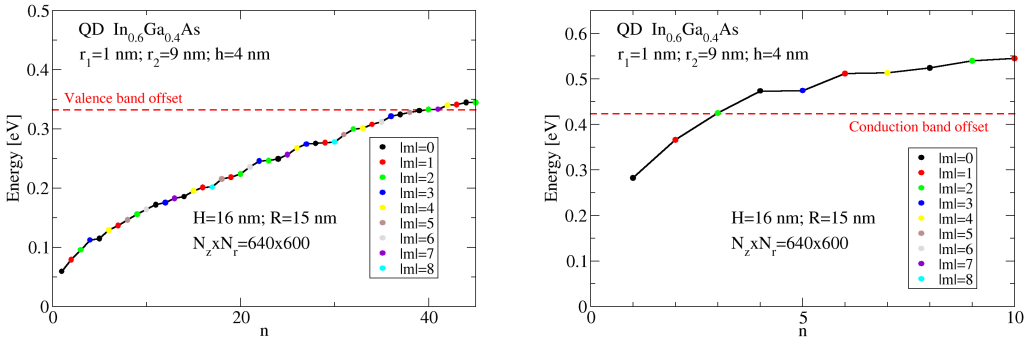

(a) Hole energies.

(b) Electron energies.

Figure 5: The eigenvalues inside a truncated cone $In_{0.6}Ga_{0.4}As$ quantum dot.

The effect of the dimensions of the virtual cylinder is evidenced in Fig. 6, together with the number of grid points. The considered values for R and H extend over the confined region (i.e. the quantum dot) with 3, 6 and 9 nm, respectively.

The bound-states (i.e. the eigenvalues under the valence band or conduction band offset) do not change with R and H. The other values, above the band offset, of course

change with R and H, because they are confined by the homogeneous Dirichlet boundary conditions inside the "virtual" cylinder with different dimensions. In order to get stable electron eigenvalues one has to consider at least $R = 18$ nm.

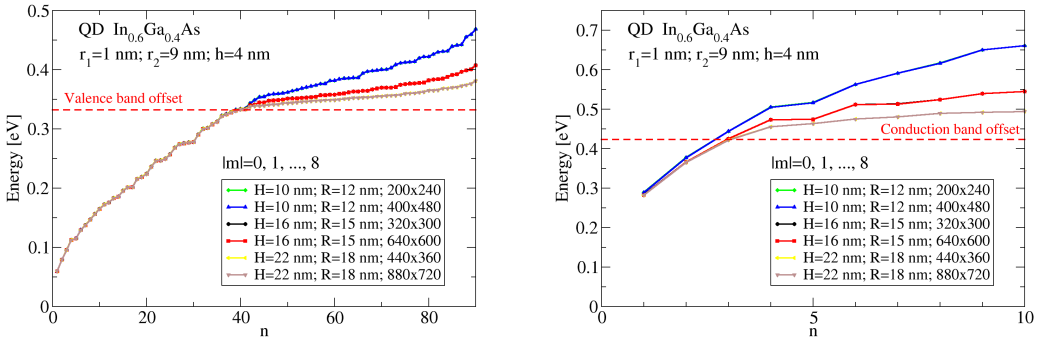

(a) Hole energies. (b) Electron energies.

Figure 6: The hole and electron eigenvalues inside a truncated cone $In_{0.6}Ga_{0.4}As$ quantum dot for different dimensions of the virtual cylinder. The grids $N_z \times N_r$ are specified in the legend.

The localization probabilities, i.e. $|\Psi(E_n; z, r)|^2$ in $[\text{nm}^{-3/2}]$ in the domain $(zr) \in [-15, 15] \times [0, 18]$, for the first four hole eigenfunctions and for the first two electron eigenfunctions (i.e. bound-states) are presented in Fig. 7 for the case $R = 18$ nm and $H = 22$ nm. They are localized inside the truncated cone. As one can see also in Fig. 5, they correspond to different m values.

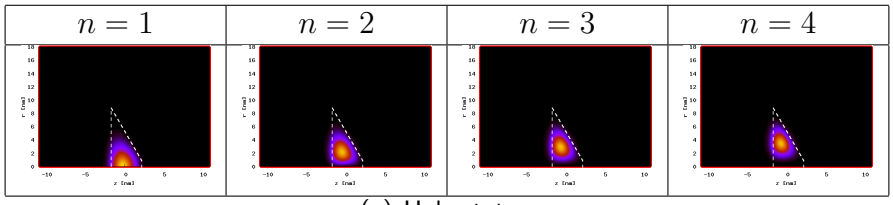

(a) Hole states.

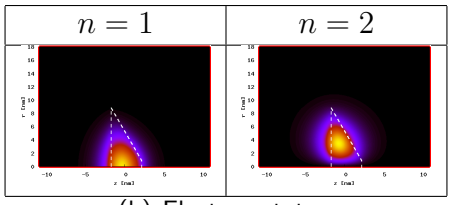

(b) Electron states.

Figure 7: Localization probabilities as (zr)-maps for the first hole and electron eigenstates in the truncated quantum dot. Bright means high values. The white lines sketch the domain of the quantum dot.

3.3 Isolated quantum well

In this section, we model the hole and electron energies inside the $In_{0.15}Ga_{0.85}As$ quantum well with the width $h_{QW} = 11$ nm.

3.3.1 Effective one-dimensional model

Fig. 8 shows the solutions of the one-dimensional effective mass Schrödinger equation for a square well potential [10, Complement H_I]. The same effective mass is considered over whole structure, namely the value for the $In_{0.15}Ga_{0.85}As$ as in Table 1, $m^* = 0.495\, m_0$ for holes and $m^* = 0.057\, m_0$ for electrons.

The eigenvalues $E_{z,i}$ obtained in the one-dimensional model are the minimum energies of the energy subbands (i.e. energy ladder) that appear in a planar nanostructure. The dispersion relation for the carriers confined in a quantum well is

$$E = E_{i,z} + \frac{\hbar^2 k_x^2}{2m_x^*} + \frac{\hbar^2 k_y^2}{2m_y^*}, \tag{14}$$

where k_x and k_y are the wave vectors in the x and y-directions that take continuous values, $k_x, k_y \in (-\infty, +\infty)$ showing the free motion in these directions.

Inside the quantum well there are at least four hole subbands and two electron subbands.

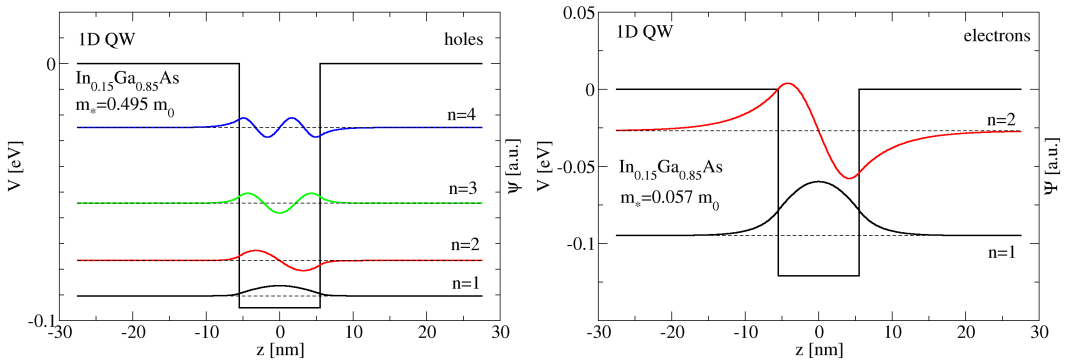

(a) holes (b) electrons

Figure 8: The eigenenergies and the real eigenfunctions for holes and electrons confined inside an one-dimensional rectangular quantum well.

3.3.2 "Quantum well" embedded inside the "virtual" cylinder

We consider a layer of $In_{0.15}Ga_{0.85}As$ embedded inside a GaAs cylinder. In our three-dimensional modeling, the quantum well is embedded inside the "virtual" cylinder. In this case, it is abusive to speak about a quantum well, because the electrons do not have two degrees of freedom for the motion inside this subsystem. They are also confined in the lateral directions (i.e. r-direction and θ-direction) so that the quantum well is *a*

quantum dot with the same radius as the nanowire, and in consequence has discrete energy spectrum.

We will consider a fixed length of the "virtual" cylinder, $H = 30$ nm. As is shown in Fig. 8, the wave functions for both electrons and holes inside the quantum well vanish at ± 15 nm. We consider three different values for R, namely $R = 12$ nm, $R = 15$ nm and $R = 18$ nm, respectively, the same as for the QD calculations. The other numerical parameters are $\texttt{mmax} = 8$ and $\texttt{nev} = 10$ for electrons and $\texttt{nev} = 30$ for holes. The mesh grid used is for all cases $h_z = h_r = 0.05$ nm.

In comparison with the previous subsection of the planar quantum well, the virtual cylinder provides a supplemental confinement, so that the energy spectrum of the carriers becomes discrete

$$E_n = E_{z,i} + E_{r,j}^{(m)}, \tag{15}$$

where $E_{r,j}^{(m)}$ are the discrete energies due to the confinement in the r-direction. They depend also on the magnetic quantum number m, due to the confinement in the θ-direction, and are given by the expression

$$E_{r,j}^{(m)} = \frac{\hbar^2}{2m_r^*} \left(\frac{x_{mj}}{R} \right)^2, \tag{16}$$

where x_{mj} is the j-th root of the Bessel function of the first kind $J_m(x)$.

The potential for the quantum well is separable, because the well extends over the whole radius of the cylinder. In turn, one can write for the eigenfunctions

$$\Psi_n(z, r) = \varphi_i(z) \xi_j^{(m)}(r). \tag{17}$$

We compute directly E_n, without writing out in explicit detail the indexes (i, j, m) for a specific n. The information about m is numerically available. The information about i and j may be obtained counting the nodes of the eigenfunctions in the z and r-direction, respectively.

In Fig. 9 are presented, in ascending order, the eigenvalues of a quantum well embedded inside the virtual cylinder. As one can see the eigenvalues are discrete. The number of eigenvalues below the valence or conduction band offsets increases with R, because the energies $E_{r,j}^{(m)}$ decrease. In the inset are shown the first eigenvalues, with respect to the first confined energy in the z-direction, $E_{z,1}$. For $R < \infty$ the eigenvalues E are larger than $E_{z,1}$ and decrease with increasing R.

Due to the cylindrical symmetry used in our model, the eigenstates for $m \neq 0$ values have a node at $r = 0$ that is not physically correct for planar quantum wells. This indicates that one should consider the eigenstates for $m = 0$ for cylinders with large R.

After the separate treatment of the subsystems, we can conclude that indeed the electron ground state in the quantum well is between the ground- and first excited state in the quantum dot, as shown in Fig. 10. With dashed lines are represented the electron eigenvalues for the one-dimensional model, while with symbols are represented the lowest eigenvalues computed within the finite volume method for the isolated quantum dot and quantum well as discussed in the previous sections.

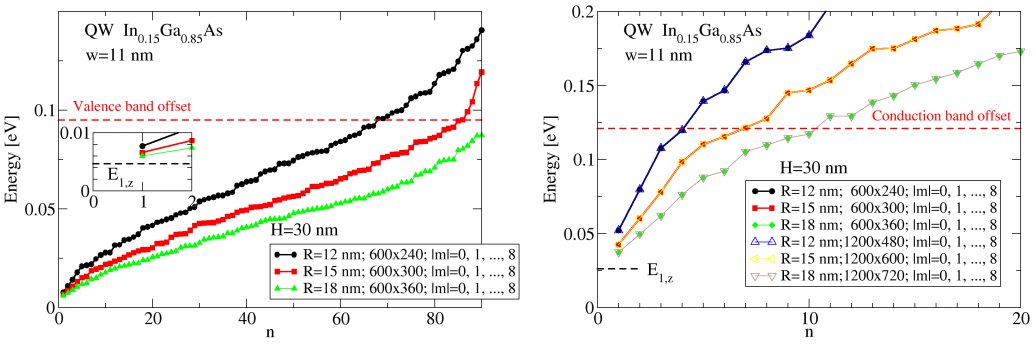

(a) Hole energies

(b) Electron energies

Figure 9: The eigenenergies for holes and electrons confined inside the quantum well of width $w = 11$ nm and embedded in the cylinder of radius R. The first confined energy in the z-direction, $E_{z,1}$, is shown in the inset with dashed line.

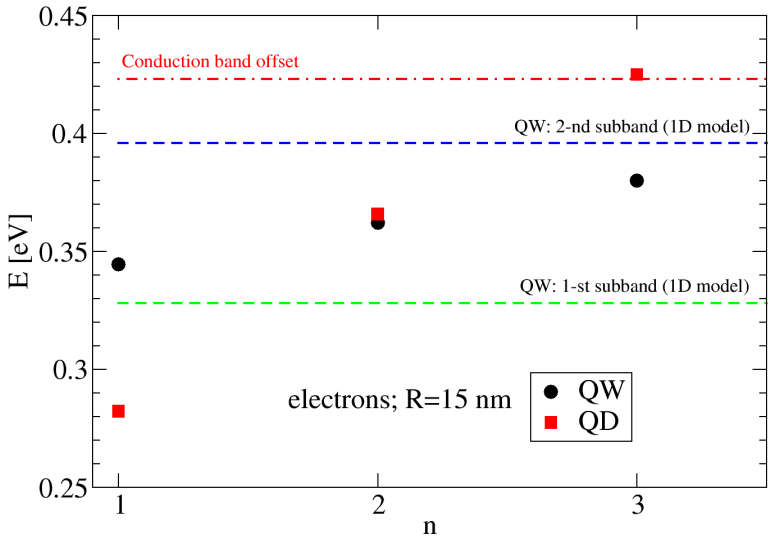

Figure 10: Comparison between the first electron states in QW and QD.

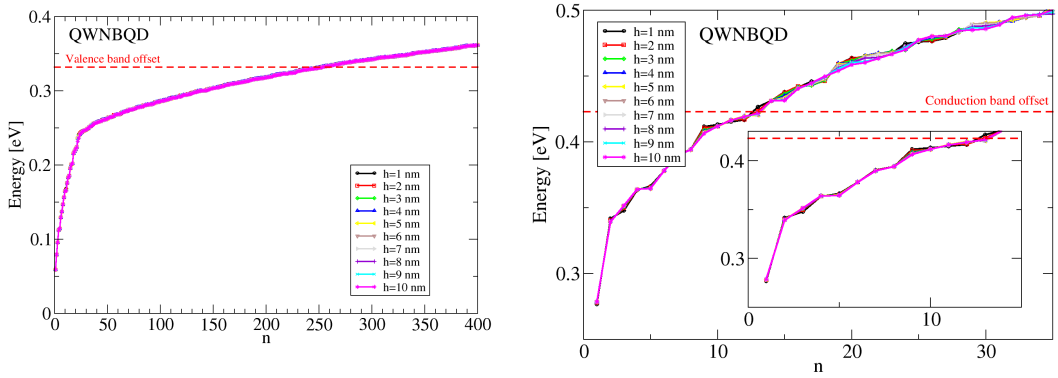

(a) Hole energies

(b) Electron energies

Figure 11: Hole and electron energies sorted in increasing order for a specific length of the nanobridge h.

3.4 Quantum well - nanobridge - quantum dot system

We consider in this section the complete system quantum well - nanobridge - quantum dot embedded inside the "virtual" cylinder. The radius and the length of the virtual cylinder are $R = 18$ nm and $H = 43$ nm, respectively. The nanobridge In content is considered linearly distributed between $x = 0.15$ and $x = 0.6$ at the ends. Different values for the length of the nanobridge are considered, $h = 1, 2, ..., 10$ nm. The numerical parameters are $\texttt{mmax} = 6$ and $\texttt{nev} = 10$ for electrons, while $\texttt{mmax} = 25$ and $\texttt{nev} = 30$ for holes. The mesh grid is $h_z = h_r = 0.05$ nm.

In Fig. 11 are presented the hole and electron energies for the complete system. As expected, there are much more hole than electron states. This is especially due to the states inside the quantum well, but there are also states localized purely inside the quantum dot.

In Fig. 12 are shown in detail the evolution of the hole states with the length of the nanobridge, i.e. the thickness of the layer between QW and QD. The energy intervals in Fig. 12 are around the values for the first and second hole states inside the isolated nanobridge, because we want to pay a particular attention to the role of the nanobridge in this complex low-dimensional structure. We marked with red ellipses the regions of crossing points between the eigenvalues. Around these crossing points *hybrid states* appear. They are localized not only in one subsystem (i.e. QW, QD or NB), but over several of them, as denoted in the last row of each table in Fig. 13. As one can see, there are hybrid states, for holes as well as for electrons, that are localized also inside the nanobridge. Notice that, the isolated nanobridge does not support localized electron states, see Sect. 3.1. The next section will establish if these hybrid states are optically active, so that they contribute to the photoluminescence spectrum.

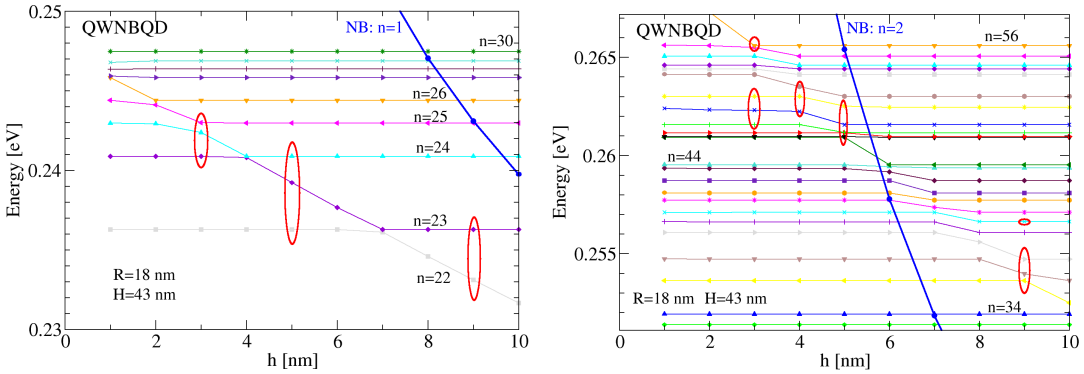

(a) (b)

Figure 12: Details of hole states from Fig. 11: around (a) the first and (b) the second localized state inside an isolated nanobridge, see Fig. 3. The red ellipses mark the regions for which hybrid states appear.

$n = 23$ $(h = 5)$	$n = 36$ $(h = 9)$	$n = 49$ $(h = 3)$	$n = 49$ $(h = 5)$
QD+NB	QD+NB	QD+NB+QW	QD+NB+QW

(a) Hole hybrid states

$n = 3$ $(h = 5)$	$n = 7$ $(h = 5)$	$n = 9$ $(h = 5)$	$n = 12$ $(h = 5)$
QD+QW	NB+QW	QD+NB+QW	QD+QW

(b) Electron hybrid states

Figure 13: Localization probabilities for some hybrid states as (zr)-maps for $z \in [-21.5, 21.5]$ nm and $r \in [0, 18]$ nm. At each state are specified the order and the h values. Bright means high values. The dashed white lines sketch the regions of QD, NB and QW. The last row in every table indicates over which regions the hybrid state extends.

4 Optical properties: oscillator strengths

In the following are presented the absolute value squared of the overlap integrals between a hole (ν = hole) state $\overline{\alpha} \equiv n_h \equiv (m_h, i_h)$ and an electron (ν' = electron) state $\overline{\alpha'} \equiv n_e \equiv (m_e, i_e)$

$$I_{\nu'\overline{\alpha'},\nu\overline{\alpha}} \simeq |\langle \psi_{n_e}, |\psi_{n_h}\rangle|^2 = \left| \int_\Omega \overline{\psi}^*_{\nu'\overline{\alpha'}}(\boldsymbol{r}) \overline{\psi}_{\nu\overline{\alpha}}(\boldsymbol{r}) d^3r \right|^2 , \tag{18}$$

called *oscillator strength*. The quantum numbers (mi) represent the magnetic quantum number m for which the two-dimensional Schrödinger-type eigenvalue problem is solved and the i is the order of the computed eigenvalue for this m value. So that these labels (mi) identify uniquely the electron or hole state. The absolute value squared of the overlap integral enters the absorption coefficient for the transition $(m_h, i_h) \rightarrow (m_e, i_e)$. Computing the absolute value squared of the overlap integrals cancels the sign uncertainty in the numerical computation of the envelope functions. For every allowed transition there is a line denoted by the indexes $(m_e, i_e; m_h, i_h)$. There are also presented the absolute value squared of the corresponding wave functions for $z \in [-15, 15]$ nm and $r \in [0, R]$ nm. The plots are given for different lengths h of the nanobridge. By changing h the absorption lines that are due to states *purely* in quantum dot or in quantum well should not change their position, while the absorption lines due to the mixed (i.e. hybrid) states change their position.

For all further calculations $H = 43$ nm and the In concentration in the nanobridge $x = 0.29$. The mesh grid is $h_z = h_r = 0.05$ nm.

4.1 $R = 18$ nm

We present first the results for $R = 18$ nm. In Fig. 14 are represented the transition lines at the corresponding transition energies together with the oscillator strengths, exemplarily for a specific h value, i.e. $h = 10$ nm. In Fig. 15 are represented the localization probabilities for the electron and hole states that contribute to the transitions.

The evolution of the transition energies (labeled as in Fig. 14) with the nanobridge length h is plotted in Fig. 16. For $h = 10$ nm, the states get well separated between the subsystems, so that it is easier to name the transition energies with respect to the subsystem in which the highest localization is. This is done in Fig. 16 for every transition line. The electron state $(0, 4)$ and the hole state $(0, 8)$ remain hybrid states for all h values, evolving from QW/QD hybrid state to a QW/NB hybrid state.

As expected, there is a weak sensitivity of the optical transitions to the length of the nanobridge [2]. Furthermore, the lowest transitions are QD-like for this combined system, because for both holes and electrons the lowest eigenstates are strongly localized inside the quantum dot.

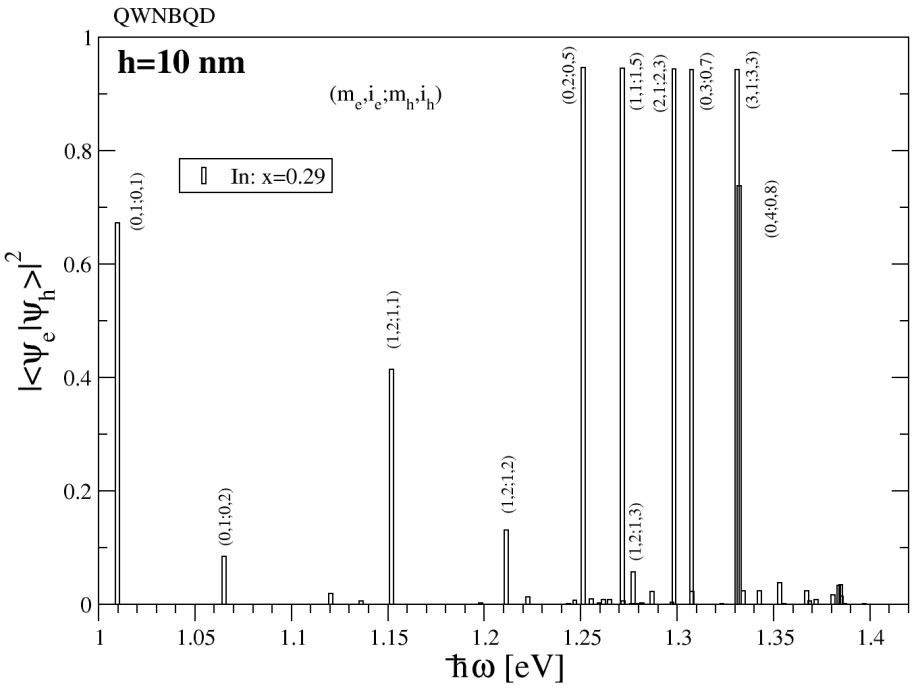

Figure 14: Transition lines together with the calculated oscillator strengths, for $R = 18$ nm.

4.2 $R = 36$ nm

Increasing the R value one gets even more electron and hole states. The lowest transition lines remain the same, reflecting the stability of the numerical calculations. The transition lines together with the oscillator strengths for $h = 10$ nm and for $R = 36$ nm are presented in Fig. 17. The evolution of the transition energies show the same weak sensibility to the h values as in the previous case. Even for this case, there exist a "hybridization" effect between two electron states, namely $(0, 5)$ and $(0, 6)$ that takes place for small h values.

In Fig. 18 are presented the transition energies together with the oscillator strengths

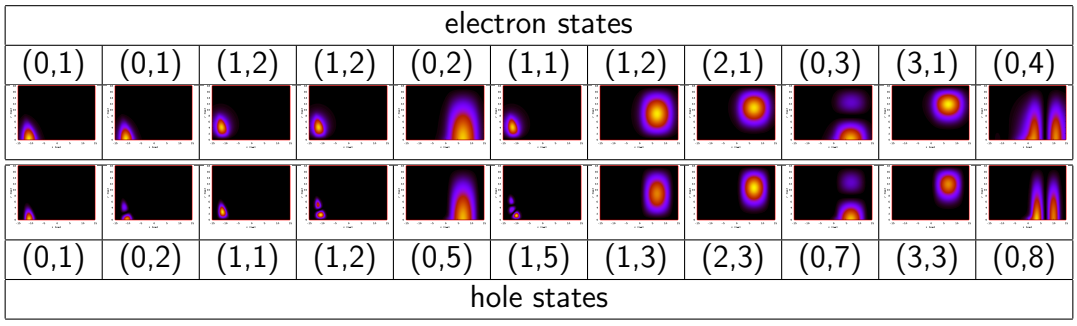

Figure 15: Localization probabilities for $z \in [-15, 15]$ nm and $r \in [0, 18]$ nm for the states contributing to the transitions in Fig. 14.

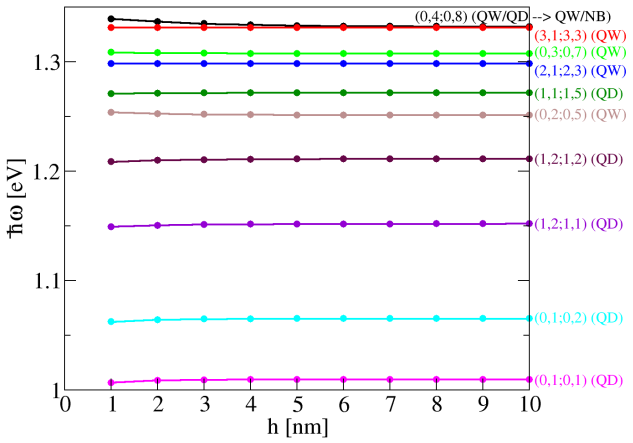

Figure 16: Transition energies versus the nanobridge length h, for $R = 18$ nm.

versus the length of the nanobridge h. The transitions $(0, 5; 0, 11)$ and $(0, 6; 0, 9)$ take place for all h values. For smaller h values, due to the "interaction" between the electron states $(0, 5)$ and $(0, 6)$ new transitions appear, namely $(0, 5; 0, 9)$ and $(0, 6; 0, 11)$. These transitions have a significant oscillator strength (i.e. higher than 0.1) and at the same time they weaken the oscillator strengths for the other two transitions. The localization probabilities for these states for $h < 6$ nm are presented in Fig. 19. One can clearly see, how the electron states $(0, 5)$ and $(0, 6)$ hybridize. For $h > 6$ nm there is no significant change in the localization probabilities of these states. One can also observe, that for $h = 1$ nm, the electron state $(0, 6)$ and the hole state $(0, 9)$ extend over QD and QW.

One can conclude that for $h \approx 5$ nm a "hybridization" phenomena [11] takes place between eigenvalues that cross and in such a way the oscillator strengths of other transition lines are weakened, producing a maximum around this h value. This may explain the additional PLE peak that appears only for certain h values [4].

4.3 $R = 54$ nm

The transition energies around 1.3 eV and the corresponding overlap integrals versus the lenght h of the nanobridge in case of $R = 54$ nm are presented in Fig. 20. One can see, that for small h values there are a few pairs of states that interact ("hybridize") and the overlap integrals get modified, such that for $h \in [4, 6]$ nm a maximum appears.

4.4 $R = 72$ nm

In case of $R = 72$ nm, the hole states $(0, 11)$ and $(0, 12)$ interact significantly for small h values. The transition energies and the corresponding overlap integrals versus the lenght h of the nanobridge are presented in Fig. 21. The overlap integral between the electron state $(0, 8)$ and hole state $(0, 12)$ gets saturated for $h > 5$ nm. The localization probabilities are presented in detail in Fig. 22.

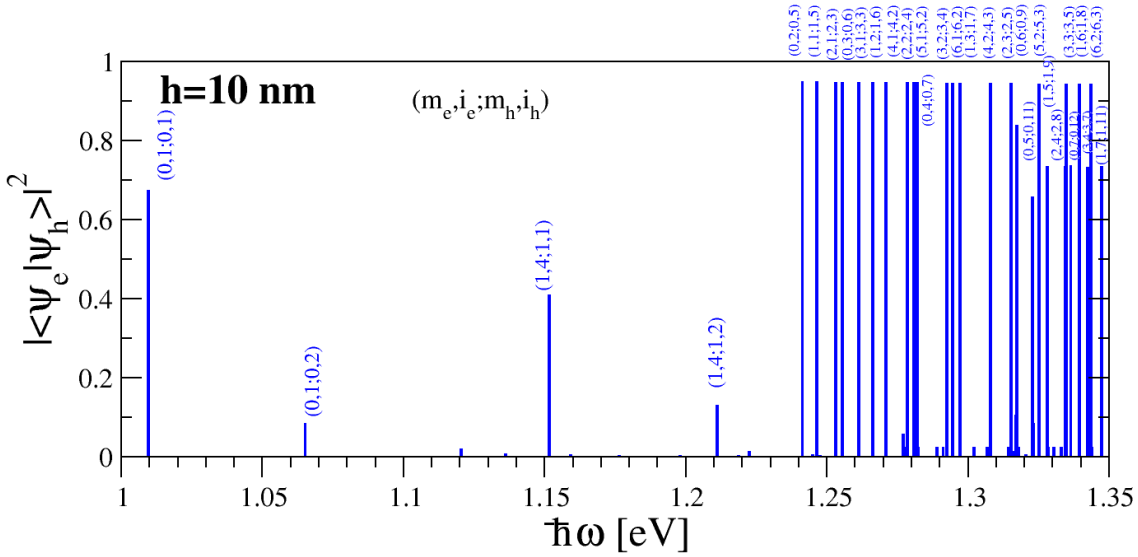

Figure 17: Transition lines together with the calculated oscillator strengths, for $R = 36$ nm.

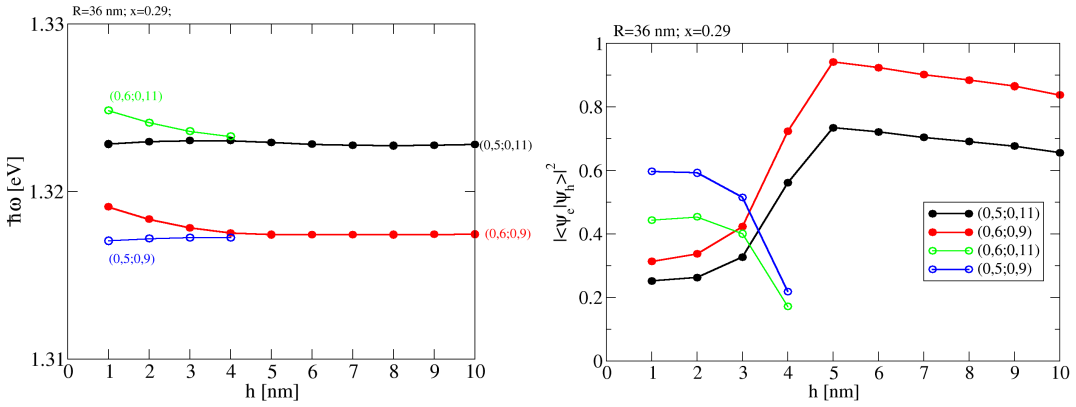

(a) Transition energies

(b) Oscillator strengths

Figure 18: Transition energies and oscillator strengths for the states that participate to the hybridization phenomena in case of $R = 36$ nm.

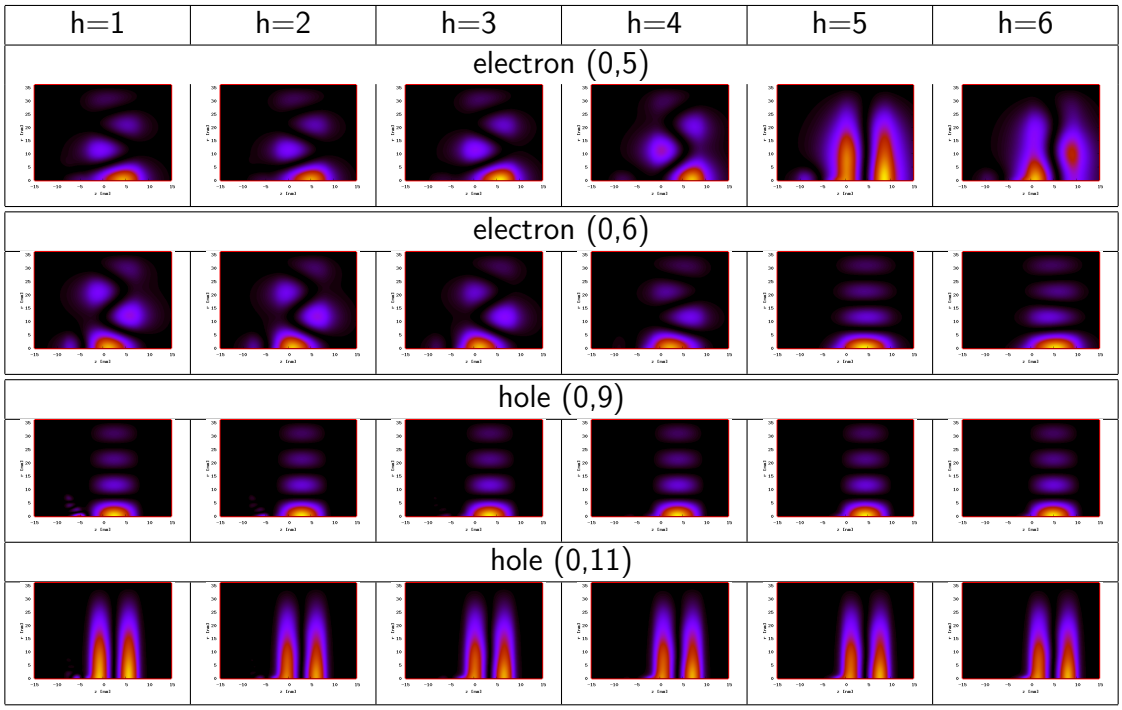

Figure 19: Localization probabilities for $z \in [-15, 15]$ nm and $r \in [0, 36]$ nm for the states that interact strongly in case of $R = 36$ nm for different lengths h of the nanobridge.

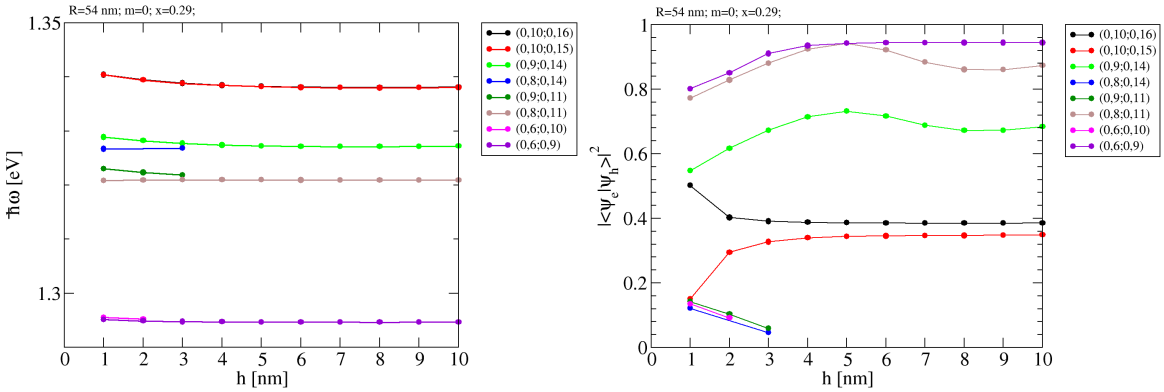

(a) Transition energies

(b) Oscillator strengths

Figure 20: Transition energies and oscillator strengths for the states that participate to the hybridization phenomena in case of $R = 54$ nm.

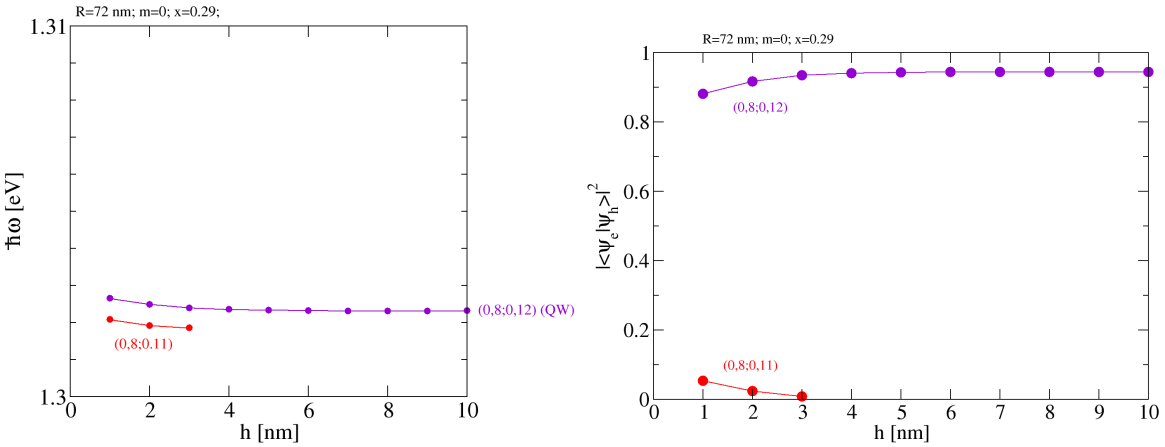

(a) Transition energies (b) Oscillator strengths

Figure 21: Transition energies and oscillator strengths for the states that participate to the hybridization in case of $R = 72$ nm.

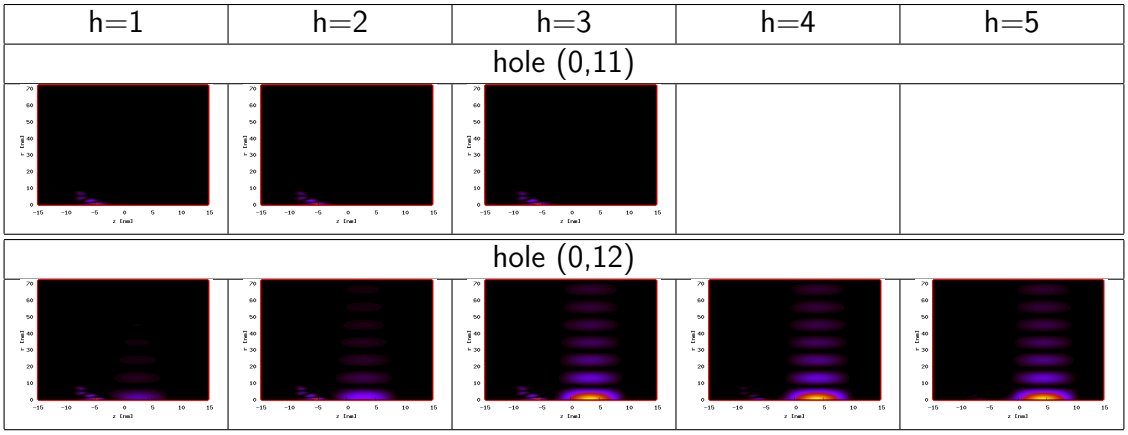

Figure 22: Localization probabilities for $z \in [-15, 15]$ nm and $r \in [0, 72]$ nm for the states that interact strongly in case of $R = 72$ nm for different lengths h of the nanobridge.

5 Conclusions

We performed electronic structure calculations within single band effective mass approximation for a complex low-dimensional structure: quantum well – nanobridge – quantum dot. In order to provide a realistic three-dimensional model, we embedded the complete system inside a "virtual" cylinder. This model yields some artefacts, even some physical features of the system are well described. We solved the eigenvalue problem within finite volume method, in order to take into account the position dependent properties of the heterostructure materials.

We reproduced the previous results for isolated nanobridge calculations. Furthermore, we computed the effect of a linear distribution of the In content inside the nanobridge. We could also check the functionality of a tunnel injection structure: the electron ground state in the quantum well is energetically between the ground and the first excited electron state in the quantum dot. For combined system states appear that extend over different subsystems, i.e. quantum well, quantum dot or nanobridge; not all of them are optically active.

The computed oscillator strengths reveal the weak sensitivity of the transition energies on the nanobridge length h. There are states that interact strongly for small distances between the quantum well and the quantum dot layers. We call this a "hybridization" phenomenon and it appears between eigenstates close to the crossing points of the eigenvalues. Moreover, due to the hybridization, the overlap integrals for some transitions get a maximum for a limited interval of h values, close to the experimental values. The "hybridization" phenomenon may be an explanation for the additional features of such structures for small h values.

6 Acknowledgments

We thank Vadim G. Talalaev and George E. Cirlin for valuable discussions concerning the experiments. We also thank Hans-Christoph Kaiser for the assistance in the numerical calculations and Valeriu Moldoveanu for valuable discussions about the modeling of optical properties.

One of us (P.N.R.) acknowledges partial support from Grant ERC-2010-AdG no.267802 AnaMultiScale from European Research Council.

A Material parameters

In this appendix we summarize the material parameters used in our modeling.

The x-dependence of the $In_xGa_{1-x}As$ material parameters are taken from [5]. The ef-

	Material	h [nm]	r [nm]	ΔE_c [eV]	ΔE_v [eV]	m_e^* [m_0]	m_h^* [m_0]
QW	$In_{0.15}Ga_{0.85}As$	11	R	0.121	0.095	0.057	0.495
QD	$In_{0.60}Ga_{0.40}As$	4	9	0.423	0.332	0.038	0.45
NB	$In_xGa_{1-x}As$	h	1	(22)	(21)	(19)	(20)
	$In_{0.30}Ga_{0.70}As$	4	9	0.232	0.182	0.050	0.480
host	GaAs	H	R	–	–	0.063	0.51

Table 1: Material parameters of the In(Ga)As/GaAs structure.

fective electron and hole masses are

$$m_e^* = \left(0.023 + 0.037(1-x) + 0.003(1-x)^2\right) m_0, \quad (19)$$

$$m_h^* = \left(0.41 + 0.1(1-x)\right) m_0, \quad (20)$$

where m_0 is the free electron mass. The band discontinuities between $In_xGa_{1-x}As/Al_yGa_{1-y}As$ are

$$\Delta E_c[eV] = \Delta E_g - \Delta E_v, \quad (21)$$

$$\Delta E_v[eV] = 0.44\,\Delta E_{gg}, \quad (22)$$

$$\Delta E_{gg}[eV] = 1.247y + 1.5x - 0.4x^2, \quad (23)$$

$$\Delta E_g[eV] = \begin{cases} \Delta E_{gg}, & \text{for } y < 0.45, \\ 0.476 + 0.125y + 0.143y^2 + 1.5x - 0.4x^2, & \text{for } y > 0.45, \end{cases} \quad (24)$$

where ΔE_{gg} is the difference between Γ-valleys in $In_xGa_{1-x}As$ and $Al_yGa_{1-y}As$. In our case $y = 0$.

References

[1] V. G. Talalaev, J. W. Tomm, N. D. Zakharov, P. Werner, U. Gösele, B. V. Novikov, A. S. Sokolov, Y. B. Samsonenko, V. A. Egorov, and G. E. Cirlin. Transient carrier transfer in tunnel injection structures. *Appl. Phys. Lett.*, 93:031105, 2008.

[2] Grzegorz Sek, Janusz Andrzejewski, Krzysztof Ryczko, Przemyslaw Poloczek, Jan Misiewicz, Elizaveta S Semenova, Aristide Lemaitre, Gilles Patriarche, and Aberrahim Ramdane. Electronic structure properties of the In(Ga)As/GaAs quantum dot-quantum well tunnel-injection system. *Semiconductor Science and Technology*, 24(8):085011, 2009.

[3] W. Rudno-Rudzinski, G. Sek, K. Ryczko, M. Syperek, J. Misiewicz, E. S. Semenova, A. Lemaitre, and A. Ramdane. Room temperature free carrier tunneling in dilute nitride based quantum well - quantum dot tunnel injection system for 1.3 um. *Appl. Phys. Lett.*, 94:171906, 2009.

[4] Alexander V. Senichev, Vadim G. Talalaev, Jens W. Tomm, Nikolai D. Zakharov, Boris V. Novikov, Peter Werner, and George E. Cirlin. Tunnel injection emitter structures with barriers comprising nanobridges. *Phys. Status Solidi RRL*, 5:385, 2011.

[5] NSM Archive - Physical properties of semiconductors. `http://www.ioffe.ru/SVA/NSM/Semicond/GaInAs/`.

[6] P. N. Racec, E. R. Racec, and H. Neidhardt. Evanescent channels and scattering in cylindrical nanowire heterostructures. *Phys. Rev. B*, 79:155305, 2009.

[7] P. N. Racec, S. Schade, and H.-C. Kaiser. Eigensolutions of the Wigner–Eisenbud problem for a cylindrical nanowire within finite volume method. *J. Comp. Phys.*, 252:52, 2013.

[8] Shun Lien Chuang. *Physics of Optoelectronic Devices*. John Wiley & Sons. Inc., New York, 1995.

[9] Fausto Rossi. *Theory of Semiconductor Quantum Devices*. Springer, Heidelberg, 2011.

[10] C. Cohen-Tannoudji, B. Diu, and F. Laloë. *Quantum Mechanics*. John Wiley & Sons, New York, 2005.

[11] E. R. Racec, U. Wulf, and P. N. Racec. Fano regime of transport through open quantum dots. *Phys. Rev. B*, 82:085313, 2010.